



# Synthesis and Characterization of Anatase $\text{TiO}_2:\text{Cu}^{2+}$ Powders Prepared via a Sol-gel Technique

Trinh Thi Loan\*, Nguyen Ngoc Long

*Faculty of Physics, Hanoi University of Science, 334 Nguyen Trai, Thanh Xuan, Hanoi*

Received 22 May 2018

Revised 23 July 2018; Accepted 01 August 2018

**Abstract:** Anatase  $\text{TiO}_2$  powders doped with different amounts of  $\text{Cu}^{2+}$  ions (0, 0.5, 1.0 and 4.0 mol%) were successfully synthesized by sol-gel method from precursors of  $\text{TiCl}_4$ ,  $(\text{CH}_3\text{COO})_2\text{Cu}$ . Effect of  $\text{Cu}^{2+}$  concentrations on the structural and optical properties of  $\text{TiO}_2$  host was investigated by X-ray diffraction, Raman spectroscopy and diffuse reflection spectroscopy. The XRD analysis showed that the doped samples exhibit anatase single phase at annealing temperature 600 °C. The  $\text{Cu}^{2+}$  contents did not affect the lattice of  $\text{TiO}_2$  host, but affected positions of its Raman modes. The band gap of the  $\text{TiO}_2:\text{Cu}^{2+}$  decreases with the increase of doping concentration.

**Keywords:**  $\text{TiO}_2:\text{Cu}^{2+}$  powders, sol-gel, structure, Raman scattering, band gap energy.

## 1. Introduction

In recent years, the titanium dioxide, also known as titania ( $\text{TiO}_2$ ), has received great attention by a lot of researchers around the world because of its potential applications, such as gas sensing [1, 2], solar cells [3], self-sterilising coatings [4], water treatment [5] and photocatalysis [6]. However, the anatase phase has a large band gap (~3.25 eV), hence the photocatalytic degradation process occurs only under ultraviolet light (less than 5 % of the solar spectrum). In the past few years, some works have been devoted to the reducing  $\text{TiO}_2$  band gap by doping  $\text{TiO}_2$  with transition metal ions. By this way, the optical response of  $\text{TiO}_2$  under visible light irradiation can improve [7]. The impurity doping induces substantial modifications in electronic structure, chemical composition and optical properties of semiconducting materials. There are many methods for synthesis of  $\text{TiO}_2$  nanomaterials such as hydrothermal, spin-on, anodic oxidative hydrolysis, sonochemical, pyrolysis routes, and sol-gel, of which, sol-gel is a simple and less expensive method.

\*Corresponding author. Tel.: 84-904367699.

Email: [loan.trinhthi@gmail.com](mailto:loan.trinhthi@gmail.com)

<https://doi.org/10.25073/2588-1124/vnumap.4272>

In this work, we synthesized the anatase  $\text{TiO}_2$  powders doped with different amounts of  $\text{Cu}^{2+}$  ions by sol-gel method. Our research was focused on the effect of  $\text{Cu}^{2+}$  dopant concentration on the crystal structure and absorption edge of anatase  $\text{TiO}_2$  powders.

## 2. Experimental

The anatase  $\text{TiO}_2$  powders doped with different amounts of  $\text{Cu}^{2+}$  ions (0, 0.5, 1.0 and 4.0 mol%) have been prepared by sol-gel method. The powders were prepared from  $\text{TiCl}_4$ ,  $(\text{CH}_3\text{COO})_2\text{Cu}$ . The aqueous solutions of  $(\text{CH}_3\text{COO})_2\text{Cu}$  and  $\text{TiCl}_4$  were mixed with the  $n_{\text{Cu}^{2+}}: n_{\text{Ti}^{4+}} = x: (1-x)$ .  $\text{C}_2\text{H}_5\text{OH}$  (98%) solution was added to the above solution. The final mixed solution was kept constant at a temperature of  $60^\circ\text{C}$  until a highly viscous gel was formed. After drying in air at  $150^\circ\text{C}$  for 24 h, the gel was converted to a xerogel more opaque and dense. The xerogel was annealed at a temperature of  $600^\circ\text{C}$  in air for 3 h.

The crystal structure of the samples was characterized by a Siemens D5005 X-ray diffractometer (XRD). Raman spectra were measured using LabRam HR800, Horiba spectrometer with 632.8 nm excitation. Diffuse reflection measurements were carried out on a VARIAN UV-VIS-NIR Cary-5000 spectrophotometer. The Kubelka-Munk (K-M) function  $F(R)$  proportional to the absorption coefficient was calculated using the equation:  $F(R) = (1-R)^2/(2R) = K/S$ , where  $R$ ,  $K$  and  $S$  are the reflection, the absorption and the scattering coefficient, respectively.

## 3. Results and discussion

To study the effects of annealing temperature and time on the formation of anatase crystalline phase, the XRD patterns of the samples doped with 4 mol%  $\text{Cu}^{2+}$  annealed at different temperature and time in air were investigated and are shown in Fig. 1. As evident from the figures, the sample annealed at  $200^\circ\text{C}$  for 3h is amorphous (line a, Fig.1). For the samples annealed at temperature of  $600^\circ\text{C}$  for 3h, nine diffraction peaks are observed at  $2\theta$  angles:  $25.3^\circ, 37.0^\circ, 38.0^\circ, 38.6^\circ, 48.0^\circ, 54.0^\circ, 55.0^\circ, 62.7^\circ$  and  $68.9^\circ$ , which are assigned to the diffraction peaks from the (101), (103), (004), (112), (200), (105), (211), (204) and (116) planes of anatase phase with tetragonal geometry, respectively (JCPDS card: 04-0477) (line b, Fig.1). When the annealing time increases to 5h, the intensity of the diffraction peaks of anatase  $\text{TiO}_2$  phase becomes stronger (line c, Fig. 1). This proves that the samples annealed at temperature of  $600^\circ\text{C}$  for 5h exhibit better crystallinity. In particular, at annealing temperature of  $700^\circ\text{C}$  for 5h, the diffraction peaks of anatase  $\text{TiO}_2$  phase are almost not observed, instead of this, the diffraction peaks of rutile  $\text{TiO}_2$  phase appear at  $2\theta$  angles:  $27.5^\circ, 36.2^\circ, 39.2^\circ, 41.4^\circ, 44.1^\circ, 54.4^\circ, 56.8^\circ, 62.8^\circ, 64.1^\circ$  and  $69.1^\circ$  (line d, Fig.1). These peaks correspond to the (110), (101), (200), (111), (210), (211), (220), (002), (310), (301) planes of rutile phase (JCPDS card: 21-1276).

Fig.2 shows the XRD patterns of  $\text{Cu}^{2+}$ -doped  $\text{TiO}_2$  with various concentrations calcined at  $600^\circ\text{C}$  for 5 h. As seen from the figure, all these samples exhibit the only anatase phase. There are no other phases such as the rutile and brookite phases of  $\text{TiO}_2$  or copper oxide phases. The undoped- $\text{TiO}_2$  samples are the white powders, meanwhile all Cu-doped  $\text{TiO}_2$  samples are pale gray one and its color becomes deeper when the concentration of Cu increases. It can be suggested that Cu ions are properly incorporated into  $\text{TiO}_2$  and uniformly distributed in lattice. Although the ionic radius of dopant  $\text{Cu}^{2+}$  ions ( $0.72 \text{ \AA}$ ) is larger than that of host  $\text{Ti}^{4+}$  ions ( $0.61 \text{ \AA}$ ), only a slight expansion of the unit cell volume could be expected due to a relatively low doping concentration. The lattice parameters and unit cell volume for the samples doped with different Cu content are calculated and shown in Table 1.

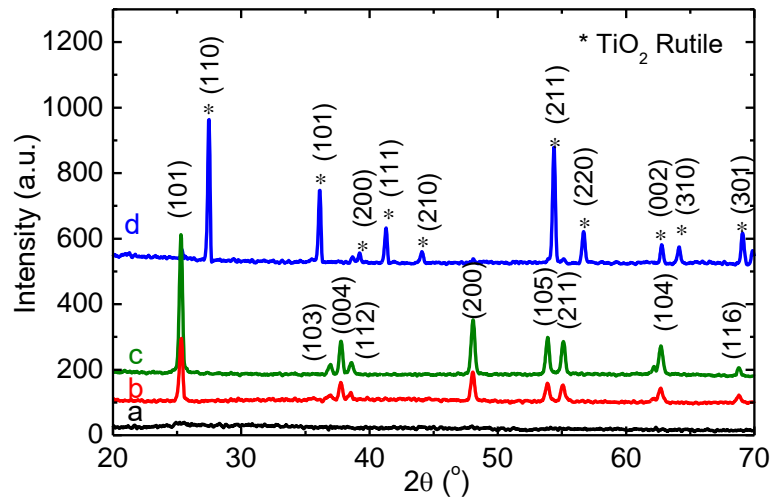


Fig. 1. XRD patterns of the samples doped with 4 mol%  $\text{Cu}^{2+}$  annealed in air at various temperatures: a- 200 °C for 3 h, b- 600 °C for 3 h, c- 600 °C for 5 h and d – 700 °C for 5 h.

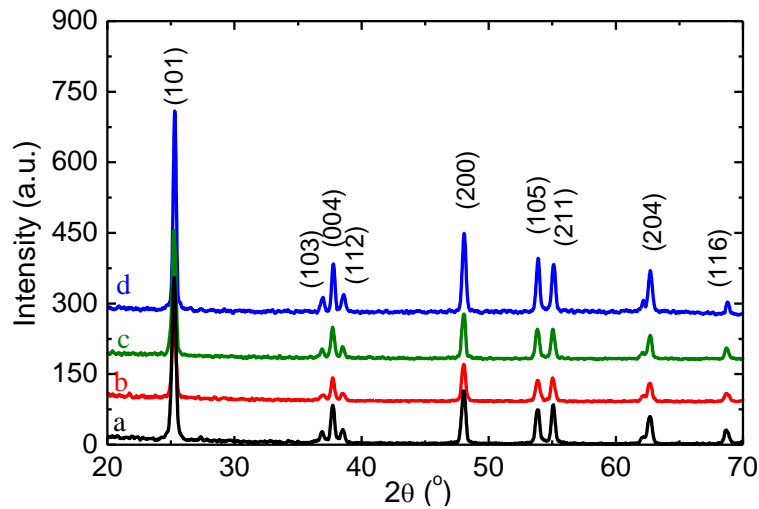


Fig. 2. XRD patterns of  $\text{TiO}_2$  doped with different amounts of  $\text{Cu}^{2+}$  ions: a- 0 mol%, b- 0.5 mol%, c- 1.0 mol%, d- 4.0 mol%.

Table 1. The average lattice parameters and unit cell volume for the samples doped with different Cu content

Samples	0 mol% Cu	0.5 mol% Cu	1.0 mol% Cu	4.0 mol% Cu
Average lattice parameters (Å)	a = 3.787 c = 9.539	a = 3.789 c = 9.545	a = 3.789 c = 9.545	a = 3.791 b = 9.539
Average unit cell volume (Å) <sup>3</sup>	136.802	137.032	137.032	137.091

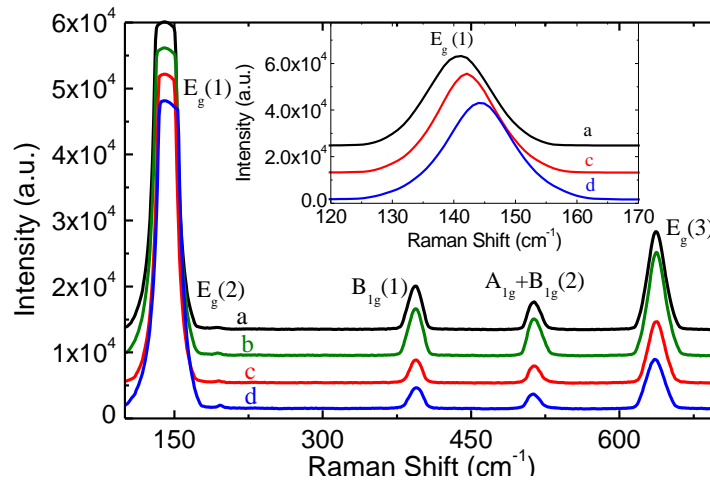


Fig. 3. Raman spectra of  $\text{TiO}_2$  doped with different amounts of  $\text{Cu}^{2+}$  ions: a- 0 mol%, b- 0.5 mol%, c- 1.0 mol%, d- 4.0 mol%.

Raman spectra of  $\text{Cu}^{2+}$ -doped  $\text{TiO}_2$  with various Cu concentrations calcined at  $600^\circ\text{C}$  for 5 h are shown in Figure 3. On each Raman spectrum are observed the  $E_g(1)$ ,  $E_g(2)$ ,  $B_{1g}(1)$ ,  $A_{1g}+B_{1g}(2)$  and  $E_g(3)$  characteristic modes for the anatase  $\text{TiO}_2$  phase [8], of which mode  $E_g(1)$  is strongest. No scattering peaks of other phases are seen, which is in good agreement with XRD analysis. The Raman vibrational modes of  $\text{TiO}_2$  are due to the symmetric, asymmetric and bending vibration of  $\text{Ti}-\text{O}-\text{Ti}$  [9]. Namely, the  $E_g$  modes are the symmetric stretching vibrations of  $\text{O}-\text{Ti}-\text{O}$  bonds. The  $B_{1g}$  modes are the symmetric bending vibrations of  $\text{O}-\text{Ti}-\text{O}$  bonds. The  $A_{1g}$  mode is the antisymmetric bending vibrations of  $\text{O}-\text{Ti}-\text{O}$  bonds [8, 9]. The frequency of Raman modes of all samples is presented in Table 2. The small difference in the positions of these Raman modes reflects the difference in the vibrational motions, which maybe due to the structural difference, namely the possible lattice distortion brought by the  $\text{Cu}^{2+}$  dopants and/ or oxygen vacancies [10].

Table 2. Raman modes of  $\text{TiO}_2$  samples doped with different amounts of  $\text{Cu}^{2+}$  ions.

Samples	$E_g(1)$ ( $\text{cm}^{-1}$ )	$E_g(2)$ ( $\text{cm}^{-1}$ )	$B_{1g}(1)$ ( $\text{cm}^{-1}$ )	$A_{1g}+B_{1g}(2)$ ( $\text{cm}^{-1}$ )	$E_g(3)$ ( $\text{cm}^{-1}$ )
0 mol%	141.1	194.2	393.6	513.4	637.1
0.5 mol%	141.1	194.5	394.0	513.4	637.1
1.0 mol%	142.2	195.1	394.4	513.0	637.4
4.0 mol%	144.4	196.3	394.8	512.5	635.4

For the determination of the band gap, diffuse reflectance spectra of synthesized samples were investigated and are shown in Fig.4A. A sharp decrease in reflectance started at about 2.98 eV for the undoped  $\text{TiO}_2$  sample due to strong absorption. The absorption edges shift to lower energy (red shift) as the  $\text{Cu}^{2+}$  concentration increases. Fig. 4B shows the Kubelka-Munk functions  $F(R)$  of the  $\text{TiO}_2:\text{Cu}^{2+}$  samples obtained from the diffuse reflection data. The band gap  $E_g$  is evaluated according to the well-known Tauc's relation [11]:

$$(ahv)^n = A(hv - E_g)$$

where  $A$  is a constant,  $\alpha$  is the absorption coefficient,  $h\nu$  is the photon energy,  $n = 1/2$  and  $2$  for the indirect and direct allowed transitions, respectively. Figs. 4C and 4D present the plots of  $[F(R) \times h\nu]^{1/2}$  and  $[F(R) \times h\nu]^2$  versus photon energy  $h\nu$  for synthesized samples, which are used to determine their indirect and direct band gap energy, respectively. For the undoped TiO<sub>2</sub> samples, we have obtained the indirect band gap of 3.24 eV and the direct band gap of 3.58 eV. These values are the same with the previously reported experimental results [7, 8, 12] and are in good agreement with the calculated values reported by Daude et al. [13] for the indirect  $\Gamma_3 \rightarrow X_{1b}$  (3.19 eV) and direct  $X_{2b} \rightarrow X_{1b}$  (3.59 eV) transitions, respectively.

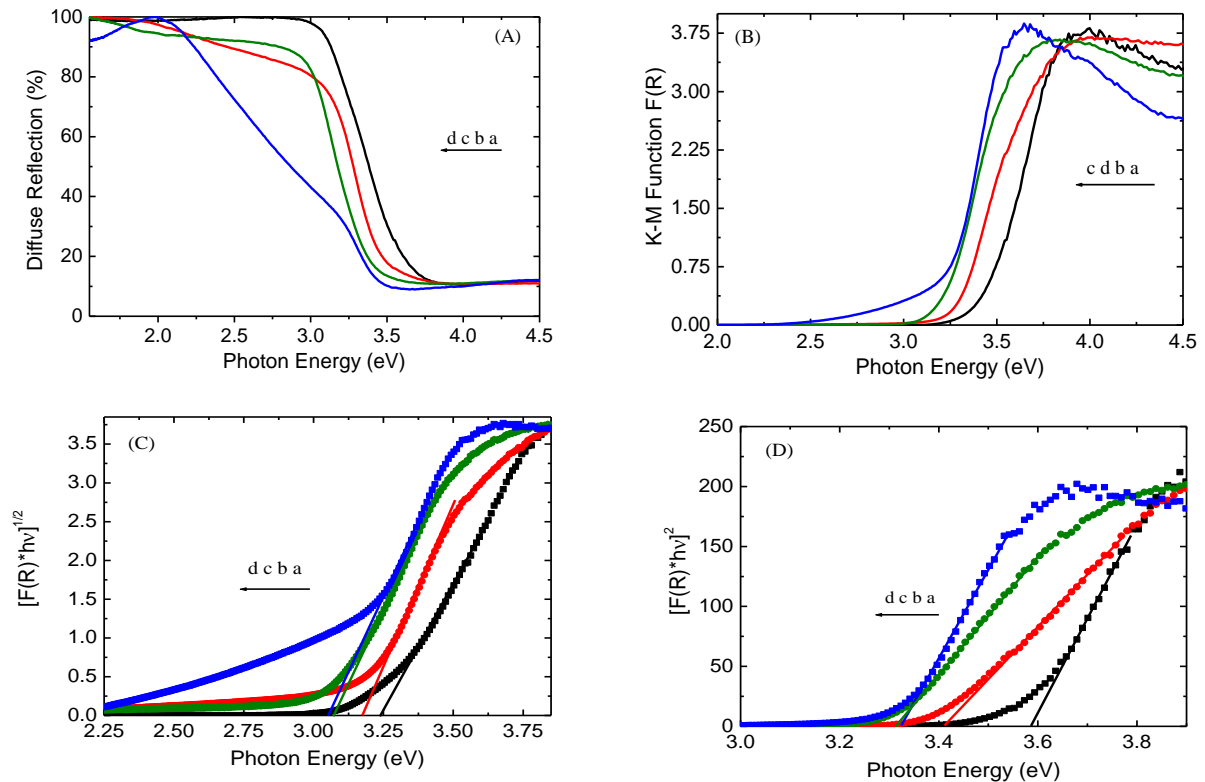


Fig. 4. (A) Diffuse reflectance spectra of TiO<sub>2</sub>:Cu<sup>2+</sup> with different Cu<sup>2+</sup> concentrations: a- 0 mol%, b- 0.5 mol%, c- 1.0 mol% and d- 4.0 mol%, (B) Kubelka-Munk functions deduced from diffuse reflectance spectra, (C) plots of  $[F(R)h\nu]^{1/2}$  and (D) plots of  $[F(R)h\nu]^2$  versus photon energy  $h\nu$ .

Table 3. Average variations of the band gap energy with Cu<sup>2+</sup>-doped TiO<sub>2</sub> samples

Cu <sup>2+</sup> content (mol%)	E <sub>g</sub> (eV)	
	Indirect transitions	Direct transitions
0	3.24	3.58
0.5	3.17	3.41
1.0	3.08	3.32
4.0	3.06	3.33

The results in Table 3 indicate that both the indirect and direct band gap of the  $\text{TiO}_2:\text{Cu}^{2+}$  decrease with the increase of doping concentration. A similar effect was observed for different transition metal ions doped in  $\text{TiO}_2$  host such as Cr [8], Zn [7], Ni [12], Fe [14]. It is well known that the valence band edge of  $\text{TiO}_2$  material is dominated by O 2p, and the conduction band edge is formed from Ti 3d [15]. Generally when transition metal ions were doped into  $\text{TiO}_2$  host, some of the new unoccupied molecular orbitals located below the conduction band of  $\text{TiO}_2$  would be formed. Therefore, the decreased band gap of the transition metal ions doped  $\text{TiO}_2$  should be likely attributed to the charge transfer from the dopant energy level of the transition metal ions to the conduction band of  $\text{TiO}_2$  or O 2p to the transition metal ions 3d instead of Ti 3d [8, 7, 12, 14]. Beside, the transition metals could also make significant changes on the electronic structure of a crystalline material and thus on the values of the gap energy [7, 8, 12].

#### 4. Conclusion

The  $\text{TiO}_2:\text{Cu}^{2+}$  powders with dopant contents 0, 0.5, 1.0 and 4.0 mol% have been successfully synthesized by sol-gel method. The XRD and Raman analysis indicated that all the synthesized samples annealed at temperature of 600 °C exhibit the anatase single phase. The lattice parameters of  $\text{TiO}_2$  host are independent on  $\text{Cu}^{2+}$  dopant content, but Raman mode positions are dependent on  $\text{Cu}^{2+}$  dopant content. The diffuse reflection spectra were used to determine both the indirect and direct band gap energy of  $\text{TiO}_2$  host as a function of the concentration of  $\text{Cu}^{2+}$  ions. The results indicated that band gap decreases with increasing  $\text{Cu}^{2+}$  dopant content.

#### References

- [1] S. Boyadjiev, V. Georgieva, L. Vergov, Z. Baji, F. Gáber and I.M. Szilágyi, *J. Phys.: Conf. Ser.* 559 (2014) 012013.
- [2] T. Xie, N. Sullivan, K. Steffens, B. Wen, G. Liu, R. Debnath, A. Davydov, R. Gomez, A. Motayed, *J. Alloys Compd.* 653 (2015) 255.
- [3] B. Roose, S. Pathak and U. Steiner, *Chem. Soc. Rev.* 44 (2015) 8326-8349.
- [4] X. Zhou, F. Chen, J. Yang, X. Yan, M. Zhong, *Mater. Sci. Eng. C*, 33 (2013) 1209–1213
- [5] S.Y. Lee, S. J. Park, *J. Ind. Eng. Chem.* 19 No. 6 (2013) 1761-1769.
- [6] J. Jia, K. Taniyama, M. Imura, T. Kanai and Y. Shigesatoa, *Phys. Chem. Chem. Phys.* 19 (2017) 17342-17348.
- [7] Trinh Thi Loan, Vu Hoang Huong, Vu Thi Tham, Nguyen Ngoc Long, *Physica B* 532 (2018) 210-215.
- [8] Trinh Thi Loan, Ngac An Bang, Vu Hoang Huong, Nguyen Ngoc Long, *Opt. Mater.* 69 (2017) 30-37.
- [9] T. Ohsaka, E. Izumi, Y. Fujiki, *J. Raman Spectrosc.* 7 (1978) 321-324.
- [10] B. Choudhury, Ranjana. Verma and A. Choudhury, *RSC Adv.* 4 (2014) 29314- 29323.
- [11] J. Tauc, R. Grigorovici, A. Vancu, *Phys. Status Solidi* 15 (1966) 627–637.
- [12] Trinh Thi Loan, Vu Hoang Huong, Tran Thi Dung, Nguyen Ngoc Long, *VNU J. Sci.: Math. – Phys.*, 32, No. 3 (2016) 34-40.
- [13] N. Daude, C. Gout, C. Jouanin, *Phys. Rev. B* 15 (1977) 3229–3235.
- [14] M.A. Ahmed, E.E. El-Katori, Z.H. Gharni, *J. Alloys Compd.* 553 (2013) 19–29.
- [15] D.O. Scanlon, C.W. Dunnill, J. Buckeridge, S.A. Shevlin, A.J. Logsdail, S.M. Woodley, C.R.A. Catlow, M.J. Powell, R.G. Palgrave, I.P. Parkin, G.W. Watson, T.W. Keal, P. Sherwood, A. Walsh, A.A. Sokol, *Nat. Mater.* 12 (2013) 798–801.